applied mechanics

MDPI

Article

On Sucker Rod Pump Systems with Data Analysis

Sheldon Wang [1,*], Clayton Brasher [1], Jimmy Tran [1], Pavle Kalaba [1] and Ty Criss [1,2]

[1] McCoy College of Science, Mathematics & Engineering, Midwestern State University, Wichita Falls, TX 76308, USA; clayton.brasher@txdot.gov (C.B.); jimmytran436@gmail.com (J.T.); pajo0411999@gmail.com (P.K.); ty@echometer.com (T.C.)
[2] Echometer Company, 5001 Ditto Lane, Wichita Falls, TX 76302, USA
* Correspondence: sheldon.wang@msutexas.edu; Tel.: +1-940-397-4061

Abstract

A sucker rod pump is an artificial lift system widely used in oil wells to extract crude oil from deep underground. Due to the clearance between the barrel and the pump plunger, a phenomenon termed slippage occurs in which the annulus column of oil returns to the pump chamber due to the plunger motion and the pressure difference at the two ends of the plunger. Although it is important to maintain the clearance for lubrication between the plunger and the pump barrel in order to prevent excessive wear and tear along with galling, excessive clearance can also be a primary factor in the reduction of oil well production and must be managed. In this research, after briefly reviewing the Couette and Poiseuille flows within the annulus region, the relaxation time for the transients, and the eccentricity effects, we focus on the derivation of important system parameters such the effective mass, stiffness, and damping ratio based on the measurements of the sucker rod displacement and the pressures or loads. Analysis of experimental measurement data can provide better understanding of the sucker rod pump system parameters, helping to quantify and manage the so-called slippage issues.

Keywords: sucker rod pump; scaling; slippage; inverse optimization; perturbation; hydraulics

1. Introduction

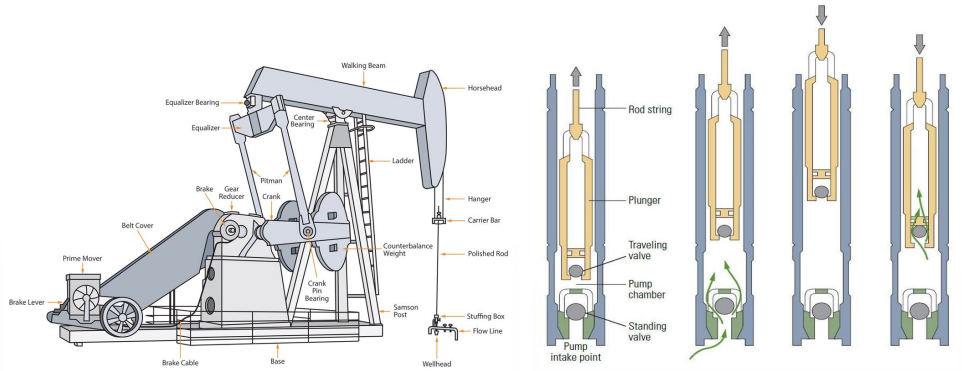
The natural lift force due to reservoir fluid pressure tends to decay over time [1]. As a result, artificial lift methods are often introduced in the oil industry. The most popular artificial lift methods consist of sucker rod pumping systems, hydraulic pumping systems, electric submersible pumping systems, and gas lift systems [2]. As one of the earliest inventions for land-based oil fields, sucker rod pumping systems have proven to be one of the most efficient, popular, and widely implemented artificial lift systems in the petroleum industry [3,4]. In fact, over 80% of the oil wells worldwide still depend on this oldest and yet extensively used mechanism [5,6]. As illustrated in Figure 1, the components of the sucker rod pump system include a long rod connected to a plunger located deep underground, typically driven by a horse-head pump jack at the surface [7]. As the mechanical lever lifts the rod string, the plunger travels upwards within the barrel, lifting a column of oil while replenishing the pump chamber. The reciprocating motion moves the sucker rod (also called the polished rod) and plunger up and down inside the well barrel [8,9]. All internal components of the sucker rod pump are enclosed within the well casing, as shown in Figure 1. The sucker rod pump system features two valves, namely, the standing and traveling valves, which open and close at different times to facilitate fluid filling in the pump chamber and transfer to the surface. As depicted in Figure 1, both

Check for updates

Received: 26 January 2026
Revised: 26 February 2026
Accepted: 18 March 2026
Published: 20 March 2026

Copyright: © 2026 by the authors. Licensee MDPI, Basel, Switzerland. This article is an open access article distributed under the terms and conditions of the Creative Commons Attribution (CC BY) license.

the plunger connecting to the polished rod and the traveling valve are located within the barrel that houses the standing valve. As the polished rod is lifted during the up stroke, the traveling valve remains closed, which keeps the standing valve open and allows the barrel to refill with fluid from oil reservoir, as shown in Figure 1. Moreover, as the well transitions from up-stroke to down-stroke, the fluid in the barrel is compressed due to the closing of the standing valve, whereas the traveling valve is opened, transferring fluid to the surface. Once the down stroke is complete, the traveling valve closes and the polished rod begins the next cycle of up- and down-stroke. Although the effectiveness and efficiency of this seemingly simple pumping mechanism have been studied for decades, there are still many engineering issues involved in this type of artificial lift systems, such as the safety and reliability of the structural materials [10,11].



(**a**) Surface mechanism (**b**) Sucker rod pump

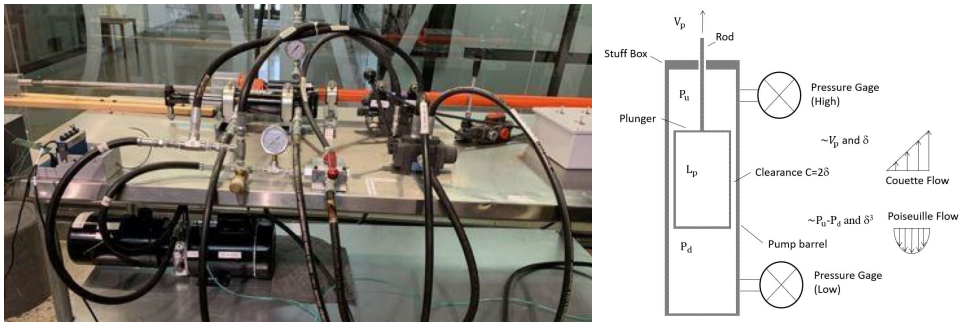
Figure 1. Well with horse-head mechanism connecting to sucker rod pump.

In this paper, we focus on production efficiency with respect to the sucker rod pump, which consists of a moving contact area between the traveling unit (the plunger, including the chamber with the so-called traveling valve), and the well tube (the barrel, which includes the so-called standing valve) [12]. Here, one mil denotes one thousandth of an inch. A clearance of 3 to 8 mils is often recommended in order to avoid direct contact or abrasion between the plunger and barrel and to allow the unimpeded passage of sand, gas bubbles, or other particles [4]. Due to the clearance between the barrel and the plunger, a so-called slippage phenomenon occurs, consisting of the annulus column of oil returning to the pump chamber due to either the pressure difference at both ends of the plunger (characterized as the Poiseuille flow) or the motion of the plunger (characterized as the Couette flow) [13,14]. It has been the goal of many researchers to quantify this slippage phenomenon and derive empirical equations related to the sucker rod pump operational parameters [15]. Again, it is important to recognize that this clearance is useful for ensuring lubrication between the plunger and the pump barrel and preventing excessive wear and tear along with galling [16]. On the other hand, an estimated 2–5% of oil is not recovered in respective daily operations [17]. In practice, it has been reported that the slippage is related to the clearance C, or two times the gap size δ, defined as the difference between the inner radius of the barrel R_i and the outer radius of the plunger R_o, in a way resembling a combined relationship of a linear and a cubic functions [18]. When dealing with sandy oil fields, the clearance is often set more than 3 mils in order to avoid abrasion and sticking [19]. In the existing literature, it has been established that in order for viscous fluid to squeeze through a narrow annulus channel, the required pressure gradient or pressure drop given a fixed plunger length L_p will be proportional to the clearance C to the power of three, namely, C^3. This derivation based on the Poiseuille flow is briefly summarized in the next section. Furthermore, the slippage issue is most prominent during the upward stroke, i.e., the sucking process. During the up-stroke, the plunger is moving upwards, and as a result

drags fluid up instead of down. This shearing effect is due to the so-called Couette flow, which introduces a flow rate in a direction consistent with the plunger's motion and proportional to the clearance C. Note that in Couette flow, we focus only on the shear flow introduced by the translational motion of the inner wall, namely, the outer surface of the plunger [14].

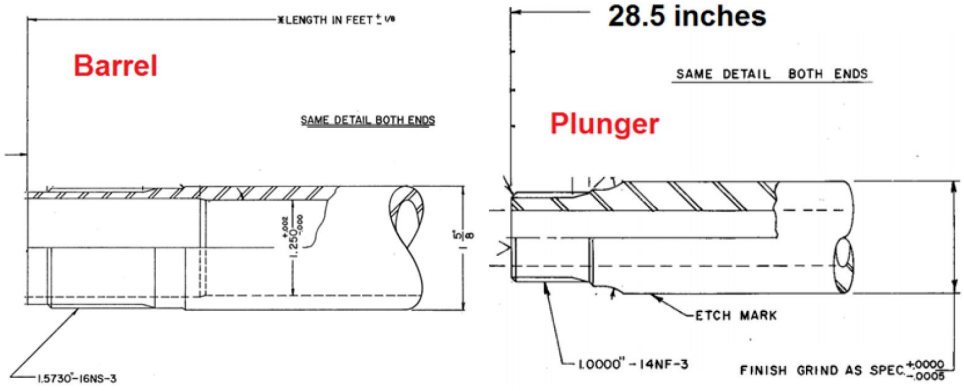
After a very concise yet self-contained review of Couette flow and Poiseuille flow as well as Bessel functions for cylinder coordinates and Fourier expansions for Cartesian coordinates, relaxation times have been estimated for transient flows within narrow annulus regions. Moreover, equivalent Cartesian coordinates have been adopted for cases with eccentricities. Earlier analytical and computational studies, verifications, and validations are also summarized. Finally, the appropriate sampling rate between 30 to 120 samples per second employed in engineering practice is confirmed to be sufficiently large in comparison with the calculated relaxation times for the transient viscous flow derived with the Bessel functions for the annulus region represented by the cylindrical coordinate system as well as its close approximation represented by the Cartesian coordinate system [13,14].

The focus of this paper is on data analysis procedures and inverse optimization methods which can be employed to obtain pump system parameters [20,21]. Over time, optimizing the performance and reliability of these pumps has become essential, especially for minimizing downtime and addressing operational inefficiencies. To facilitate the study of sucker rod pump systems, an experimental setup with both horizontal and vertical configurations, as illustrated in Figures 2 and 3, has been established at the McCoy School of Engineering at MSU Texas, a member of the Texas Tech university system, utilizing a Linear Variable Differential Transformer (LVDT) sensor (OMEGA Model LD620-25, M930415AK12-02, 102 Indiana Hwy. 212, Michigan City, IN 46360, USA) connected with National Instrument (NI) LabVIEW software (Version 2018, 11500 N Mopac Expwy, Austin, TX 78759, USA) and a set of two pressure gauges connected with Echometer Total Asset Monitor (TAM) software (Version 2.0, 5001 Ditto Lane, Wichita Falls, TX 76302, USA). The LVDT is strategically mounted next to the end of the plunger to provide precise and real-time measurements of its displacement throughout the pump's cycle. By obtaining accurate displacement data along with pressure measures, it is possible to calculate key system parameters using our proposed mathematical models [7,22]. In today's engineering environment, many of the system parameters can be derived through measurements and inverse optimization procedures [23,24]. In fact, with artificial intelligence (AI), this type of data analysis is expected to become more effective in comparison with the traditional first principle based direct measurements. The experimental setup we have established at the McCoy School of Engineering at MSU Texas will also be studied with different focuses in the near future, for example through the calibration of the LVDT's internal mass and stiffness. With better mathematical models and associated system parameters derived with and confirmed by our in-house sucker rod pump system experimental setup, better understanding and management of the slippage issue can also be accomplished.



(**a**) Actual System (**b**) Illustration

Figure 2. McCoy School of Engineering sucker rod pump experimental setup (adopted from [15]).



(**a**) (**b**)

Figure 3. Design details of the solid plunger and the barrel.

2. Poiseuille and Couette Flows

In this section, we summarize the Poiseuille flow and Couette flow related to the slippage issues as well as the relaxation time for the transient flow and eccentricity effects. Taking into consideration the excessively small gap or clearance in comparison with the barrel or plunger radius (often on the order of a few mils), we have compared and confirmed the matching of the relaxation times predicted with Bessel functions for cylindrical coordinates and those with Fourier expansions for Cartesian coordinates. We have also compared the largest relaxation time with the sampling rate, which is around 30 to 120 samples per second, for engineering practice and our experimental measurements. This comparison confirms that the quasi-static assumption in the field is sufficiently accurate and appropriate, as reported in [13,14]. Consider a pump system with the outer radius R_o of the plunger and inner radius R_i of the barrel. The gap, denoted as $\delta = R_i - R_o$, is small in comparison with the plunger's outer radius R_o and length L_p. Both the Poiseuille flow due to the pressure difference and the Couette flow due to the plunger's motion are considered as two linear viscous solutions which can be superimposed. As illustrated in Figures 1–3, the plunger is closely fitted within the pump barrel. In general, there will be a clearance of 3 mils for a typical oil well. Moreover, the friction force between the plunger and the barrel is due to viscous shear instead of Coulomb friction through direct contact or abrasion.

In this paper, we adopt a uniform notation consistent with our own experimental setup. As the plunger is lifted up, the pressure difference $p_u - p_d$ or the pressure gradient $(p_u - p_d)/L_p$, with L_p as the plunger's axial length, will drive the fluid from the high-pressure area, that is, the top of the plunger (also called the rod side or up-chamber) to the low-pressure area, that is, the bottom of the plunger (also called the cap side or down-chamber). Note that the so-called slippage is due to both Poiseuille flow and Couette flow

within the annulus region; more specifically, the slippage direction is often referred to by the direction. Slippage from the top of the plunger to the pump chamber or the bottom of the plunger is aligned with the Poiseuille flow velocity when the plunger is lifted up [25]; the other contribution to the slippage is due to Couette flow within the same annulus region, which is introduced by the plunger's motion. It is important to recognize that during the up- and down-stroke, the Couette part of the slippage is in the same direction of the reciprocal plunger motion.

During the operation of the sucker rod pump systems, as illustrated in Figures 1–3, two fundamental fluid flows exist within the gap between the plunger outer surface and the barrel inner surface, one the pressure difference-driven Poiseuille flow, and the other the boundary motion-induced Couette flow. Couette flow is a steady-state, incompressible, and one-dimensional viscous fluid flow through two parallel plates with different velocities. The fluid motion is due to the moving surface's dragging effect on the surrounding fluid due to the fluid viscosity with a so-called no-slip condition. In our system, as depicted in Figure 4, the highest velocity of Couette flow occurs adjacent to the moving outer surface of the plunger with velocity V_p, which is determined by the above-ground polished rod motion along with the kinematic conditions $v(R_i) = 0$ and $v(R_o) = V_p$. Consequently, the viscous force F_c acting on the plunger will be in the opposite direction to the plunger velocity V_p, whereas the induced volume flow rate Q_c will be in the same direction.

On the other hand, due to the pressure difference $\Delta p = p_u - p_d$ or the pressure gradient in the axial direction from the up-chamber to the down-chamber, namely, $\partial p/\partial z = -(p_u - p_d)/L_p$ with the plunger length L_p, the Poiseuille flow direction is aligned with the pressure gradient direction so that the viscous shear force F_p acts on the plunger's outer surface and the volume flow rate Q_p, as shown in Figure 4. Again, for the Poiseuille flow, we have the kinematic conditions $v(R_o) = 0$ and $v(R_i) = 0$ on the surfaces of the pump barrel and the plunger, respectively. Note that both the Poiseuille and Couette flows are idealized quasi-static or steady laminar flows. According to the specific geometries of typical sucker rod pump systems and their operating conditions, we may first ignore the inertial and time dependent effects and focus on the steady-state effects. Hence, the Navier–Stokes equation in the cylindrical coordinate system can be simplified as a combination of the Poiseuille flow and Couette flow, governed by the following equations:

$$0 = -\frac{\partial p}{\partial z} + \mu \frac{1}{r}\frac{\partial}{\partial r}\left(r\frac{\partial v}{\partial r}\right) \tag{1}$$

with z as the axial direction coordinate and v the axial direction fluid velocity.

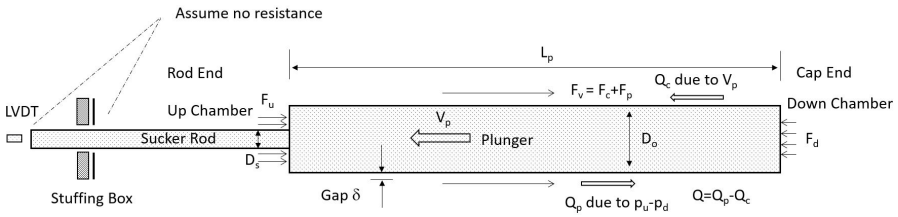


Figure 4. Plunger external loads and respective volume flow rates of the sucker rod experimental validation system model (adopted from [15]).

For the Couette flow, we have $\Delta p = 0$. Therefore, the flow field is expressed as

$$v(r) = C_1 \ln r + C_2, \tag{2}$$

with $C_1 = -V_p/(\ln R_i - \ln R_o)$ and $C_2 = V_p \ln R_i/(\ln R_i - \ln R_o)$.

Using Taylor expansion with the small gap assumption, we have the following simplified expression for the Couette flow field:

$$v(r) = \frac{V_p R_o}{\delta}(\ln R_i - \ln r). \tag{3}$$

Notice that the gradient of the velocity profile at the plunger surface matches the approximation with respect to the thin gap. Moreover, the Couette flow rate Q_c for the annulus region can still be written as $\int_{R_o}^{R_i} 2\pi v(r) r dr$, which is in the same direction as the plunger velocity V_p, that is, from the down-chamber to the up-chamber, as stipulated in Figure 4. Using Taylor expansions, as elaborated in [14], we have

$$Q_c = \pi V_p R_o^2 (\epsilon + \frac{7}{6}\epsilon^2 + \frac{11}{12}\epsilon^3 + \frac{5}{72}\epsilon^4 - \frac{13}{48}\epsilon^5). \tag{4}$$

The expression in Equation (4) matches the approximation of similar Couette flow results in rectangular domains. As a consequence, the viscous shear force F_c acting on the plunger's outer surface in the direction from the up-chamber to the down-chamber, which is opposite to the Couette flow direction defined by the sucker rod velocity V_p, can be calculated as

$$F_c = -2\pi R_o L_p \mu \frac{\partial v}{\partial r}\bigg|_{r=R_o} = \frac{2\pi L_p \mu R_o V_p}{\delta}(1 + \frac{1}{2}\epsilon - \frac{1}{12}\epsilon^2 - \frac{5}{24}\epsilon^3 - \frac{11}{144}\epsilon^4 + \frac{1}{32}\epsilon^5). \tag{5}$$

In fact, the viscous shear force F_c acting on the plunger's outer surface due to the Couette flow is opposite to the direction of the plunger's motion V_p, defined as positive from the down-chamber to the up-chamber, and the estimate in the expression in Equation (5) matches the simple approximation based on thin fluid layers as discussed in [13]. Likewise, for the Poiseuille flow, the velocity profile within the annulus region expressed as Equation (2) has the following coefficients:

$$C_1 = \frac{\Delta p}{4\mu L_p}\frac{R_i^2 - R_o^2}{\ln R_i - \ln R_o} \text{ and } C_2 = \frac{\Delta p}{4\mu L_p}(R_o^2 - \frac{R_i^2 - R_o^2}{\ln R_i - \ln R_o}\ln R_o).$$

Using the assumption of small clearance and Taylor expansion, following the derivation in [14] for the Poiseuille flow gives us

$$v(r) = -\frac{\Delta p}{4\mu L_p}\Big(-r^2 + 2R_o^2 \ln r + R_o^2 - 2R_o^2 \ln R_o\Big), \tag{6}$$

where both Dirichlet velocity boundary conditions are satisfied at annulus surfaces with $r = R_o$ and $r = R_i$, respectively.

Within the annulus region, we can easily establish the Poiseuille flow rate Q_p as $\int_{R_o}^{R_i} 2\pi v(r) r dr$. It is not too difficult to confirm that up to $o(\delta^2)$, the flow rate due to the pressure difference Q_p is indeed zero. At $o(\delta^3)$ we can establish the Poiseuille flow rate with $\epsilon = \delta / R_o$, as follows:

$$Q_p = \frac{\pi \Delta p}{6\mu L_p} R_a^4 (\epsilon^3 + \frac{1}{2}\epsilon^4 - \frac{11}{15}\epsilon^5). \tag{7}$$

Consequently, the viscous shear force F_p acting on the plunger's outer surface due to the pressure gradient in the direction from the up-chamber to the down-chamber can be calculated as

$$F_p = 2\pi R_o L_p \mu \frac{\partial v}{\partial r}\bigg|_{r=R_o} = \pi \Delta p R_o^2 (\epsilon + \frac{1}{6}\epsilon^2 - \frac{1}{4}\epsilon^3 - \frac{13}{72}\epsilon^4 - \frac{1}{144}\epsilon^5). \tag{8}$$

Notice that the viscous shear force F_p acting on the plunger's outer surface is consistent with the Poiseuille flow direction; the leading term in Equation (8) represents the half of the total normal force difference, attributed to the pressure difference, acting on the fluid within the annulus region [14].

3. Time Scales and Perturbations

To further investigate the inertia effects, which are essential for the selection of sampling rates, we consider the overall governing equation for the viscous flow within the annulus region with $R_o \leq r \leq R_i$ expressed as

$$\rho \frac{\partial v}{\partial t} = -\frac{\partial p}{\partial z} + \mu \frac{1}{r} \frac{\partial}{\partial r}(r \frac{\partial v}{\partial r}), \tag{9}$$

where the fluid density is ρ, the axial z direction is consistent with the direction of the flow with the plunger length L_p, and the pressure gradient $\partial p/\partial z$ is expressed as $-\Delta p/L_p$ or $-(p_u - p_d)/L_p$.

Note that the pressure difference Δp is positive when the pressure in the upper region is higher than that in the lower region, which is consistent with the slippage definition. Assuming that the plunger velocity is V_p, that is, $v(R_o) = V_p$, by combining the Couette flow and Poiseuille flow we can arrive at the steady-state solution for the velocity profile $\phi(r)$, expressed with $\delta = C/2$ as follows:

$$\phi(r) = \frac{1}{4\mu} \frac{\Delta p}{L_p} \left(r^2 - \frac{R_i^2 - R_o^2}{\ln R_i - \ln R_o} \ln r - \frac{R_o^2 \ln R_i - R_i^2 \ln R_o}{\ln R_i - \ln R_o} \right) + \frac{V_p(\ln R_i - \ln r)}{\ln R_i - \ln R_o}. \tag{10}$$

It is important to point out that the plunger velocity V_p is negative when it is moving downwards, which is also consistent with the slippage definition. The final unsteady velocity profile $v(r,t)$ can be written as $v(r,t) = \phi(r) - \bar{v}(r,t)$, where the steady-state solution is expressed as $\phi(r)$, as stipulated in Equation (10), and the governing equation for the transient part $\bar{v}(r,t)$ can be written as follows (with boundary conditions $\bar{v}(R_o,t) = 0$ and $\bar{v}(R_i,t) = 0$):

$$\frac{\partial \bar{v}}{\partial t} = \nu \frac{1}{r} \frac{\partial}{\partial r}(r \frac{\partial \bar{v}}{\partial r}). \tag{11}$$

Using the separation of variables method and common special functions [26], we introduce $\bar{v}(r,t) = \psi(t)\varphi(r)$. As a consequence, we have $\varphi(R_o) = \varphi(R_i) = 0$ and the following governing equations in the cylindrical coordinate system:

$$\begin{aligned} \dot{\psi} + \frac{\psi}{\tau} &= 0, \\ \frac{1}{r}\frac{d}{dr}(r\frac{d\varphi}{dr}) + \frac{1}{\nu\tau}\varphi &= 0, \end{aligned} \tag{12}$$

where ν is the kinematic viscosity and the time scale τ is also called the relaxation time.

In general, for an exponential increase or decrease function expressed as $e^{-t/\tau}$, the tangent line at the origin always provides an horizontal intercept τ, and the function will approach the steady-state solutions within 5–6 times the relaxation time τ. From Equation (12), we have $\psi(t) = A_o e^{-t/\tau}$ and the characteristic expression for $\varphi(r)$ is $A_1 J_o(\sqrt{\frac{1}{\nu\tau}} r) + A_2 Y_o(\sqrt{\frac{1}{\nu\tau}} r)$, where the characteristic time τ is determined by the boundary conditions of $\varphi(r)$, namely, $\varphi(R_o) = \varphi(R_i) = 0$, along with Bessel functions of the first and second kinds J_o and Y_o, respectively. Therefore, in order to have nontrivial solutions of coefficients A_1 and A_2 for the set of equations

$$\begin{aligned} A_1 J_o(\sqrt{\tfrac{1}{\nu\tau}} R_o) + A_2 Y_o(\sqrt{\tfrac{1}{\nu\tau}} R_o) &= 0, \\ A_1 J_o(\sqrt{\tfrac{1}{\nu\tau}} R_i) + A_2 Y_o(\sqrt{\tfrac{1}{\nu\tau}} R_i) &= 0, \end{aligned}$$

the determinant of the coefficient matrix must be zero, namely,

$$det(\tau) = J_o(\sqrt{\frac{1}{\nu\tau}} R_o) Y_o(\sqrt{\frac{1}{\nu\tau}} R_i) - J_o(\sqrt{\frac{1}{\nu\tau}} R_i) Y_o(\sqrt{\frac{1}{\nu\tau}} R_o) = 0. \tag{13}$$

Finally, the velocity profile can be expressed as $v(t,r) = \phi(r) - \sum_{k=1}^{\infty} A_k e^{-t/\tau_k} g_k(r)$, where the special function can be expressed as

$$g_k(r) = J_o(\sqrt{\frac{1}{\nu\tau_k}} r) Y_o(\sqrt{\frac{1}{\nu\tau_k}} R_o) - J_o(\sqrt{\frac{1}{\nu\tau_k}} R_o) Y_o(\sqrt{\frac{1}{\nu\tau_k}} r) \tag{14}$$

and the coefficient A_k is calculated as $A_k = \int_{R_o}^{R_i} \phi(r) g_k(r) r dr / \int_{R_o}^{R_i} g_k(r)^2 r dr$.

Consider a practical case with $R_o = 0.75$ in and $C = 5$ mils along with measured plunger velocity around 40 in/s, namely, $\delta = C/2 = 0.0025$ in. For the fluid considered in this paper, we assume that the density ρ is about 1.0014×10^3 kg/m^3 and the plunger length $L_p = 4$ ft. Let us first evaluate the Reynolds numbers. Assuming that the dynamic viscosity for our example is 0.9867 cp, we have the Reynolds number based on the plunger diameter $2\rho R_o V_p/\mu$ as 39,286, which suggests that the flow pattern on top of the plunger can be turbulent. Thus, three-dimensional computational fluid dynamics (CFD) modeling tools must be utilized. On the other hand, the Reynolds number based on the clearance $\rho C V_p/\mu$ is 130.954, which demonstrates that the viscous flows within the annulus region are laminar.

In order to further demonstrate this point about the relaxation time, we employ the perturbation approach utilizing the extreme condition when the plunger radius R_o is much large than the gap size δ. As elaborated in [13,26], the two-dimensional governing equation expressed in the cylindrical coordinate system (11) can be expressed in the equivalent Cartesian coordinate system with y in the thickness direction as follows:

$$\frac{\partial \bar{v}}{\partial t} = \nu \frac{\partial^2 \bar{v}}{\partial y^2} \tag{15}$$

with the same Dirichlet boundary conditions $\bar{v}(R_o, t) = 0$ and $\bar{v}(R_i, t) = 0$.

Using the same separation of variable method as stipulated in [14], we introduce $\bar{v}(y,t) = \psi(t)\varphi(y)$. As a consequence, we have $\varphi(R_o) = \varphi(R_i) = 0$, and the governing equations in the equivalent Cartesian coordinate system are

$$\begin{aligned} \dot{\psi} + \frac{\psi}{\tau} &= 0, \\ \frac{d^2\varphi}{dy^2} + \frac{1}{\nu\tau}\varphi &= 0. \end{aligned} \tag{16}$$

From Equation (16) and the corresponding boundary conditions, we can easily obtain the sinusoidal expansion of the function $\varphi(r)$ with the half-period δ, namely, $\sin(\frac{n\pi}{\delta} y)$, with the modal sequence number n. Moreover, from Equation (16) we have

$$n = \frac{\delta}{\pi} \frac{1}{\sqrt{\nu\tau}}. \tag{17}$$

As a consequence, Equation (17) can be used to de-dimensionalize the relaxation times τ and perform confirmation using the roots derived from on the corresponding Bessel functions of the first and second kinds [13,14]. Hence, we have the graphical representation shown in Figure 5 for the determinant expressed in Equation (13). The eigensolutions α_k with $k = 1, 2, \cdots$ relate to the non-dimensional characteristic time or relaxation time $\tau_k = \delta^2/(\pi^2 \nu \alpha_k^2)$. In this case, we have the largest characteristic time $\tau_1 = 4.1464 \times 10^{-1}$ ms. Furthermore, ξ_n evaluated by the roots in Figure 5 can be simply expressed as $1/n^2$. This observation confirms that by simplifying the Bessel functions using the sinusoidal functions as $R_o/\delta \to 0$, it is clear that the typical sampling period of 8.333 ms is sufficiently larger than five or six times the largest intrinsic relaxation time, as predicted in Figure 5. Therefore, the transient or time-dependent effects can be ignored and quasi-static analytical approaches can be adopted. Furthermore, we have an evaluation of the largest relaxation time τ expressed with the mode number $n = 1$, $\tau = \delta^2/(\pi^2 \nu)$. In the early computational simulation we applied the pressure differential for three out of four strokes, namely, 1295 sample points or 10.7917 s, leaving only the stroke during which both the traveling valve (TV) and the standing valve (SV) are closed. Notice that in this test case we have the stroke per minute (SPM) as 5.0669; thus, the period of the sucker rod pumping unit is about 11.8417 s. In order to be consistent with the rate of 120 sampling points per second, a sampling step size of 8.333 ms is also adopted. To keep the units consistent, the pressure unit is psi, and the dynamic viscosity unit is psi · s. However, since the spatial dimension is represented with in, conversion factors of 32.147 for the gravitational constant and 12 for foot and inch conversion must be adopted in the left-hand side (LHS) of the Navier–Stokes equation, which means that the density must be adjusted accordingly in addition to the standard conversion from kg/m^3 and lbm/ft^3. Therefore, the actual input to computational programs if the dimensions are in inches and the pressure differentials are in psi are 9.3583×10^{-5} for effective density and 14.5045×10^{-8} for effective dynamic viscosity.

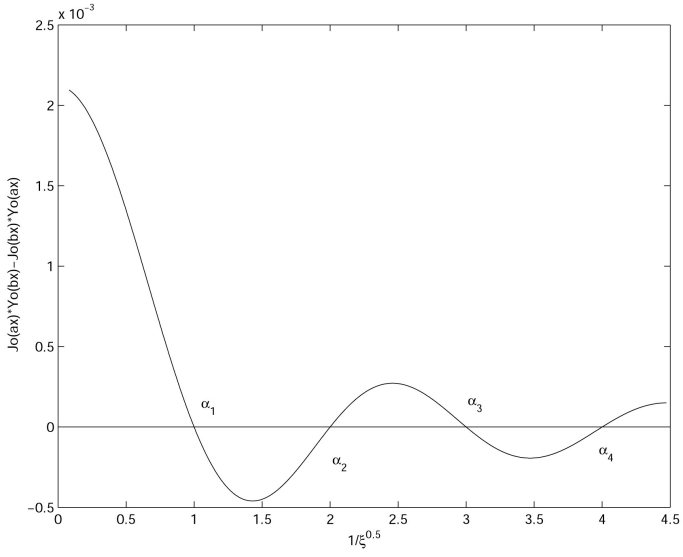


Figure 5. Eigensolutions of the characteristic function and the characteristic time with $a = \sqrt{\frac{1}{\nu}} R_o$, $b = \sqrt{\frac{1}{\nu}} R_i$, $\sqrt{\xi} = \sqrt{\tau}\pi\sqrt{\nu}/\delta$, and $x = (\sqrt{\nu}\pi)/(\delta\sqrt{\xi})$ (adopted from [14]).

Finally, to incorporate the eccentricity effects as elaborated in [13,14], we denote e as the shift of the center of the inner cylinder; hence, the eccentricity is measured by $2e/C$. As discussed in [13,14], the eccentricity of the plunger's lateral position in the barrel has a significant effect on viscous flows within the annulus region as well as the respective leakages. Again, to approximate the cylindrical coordinate system with an equivalent Cartesian

coordinate system, we cut the perimeters along the radial directions aligned with the narrowest gap and express half of the perimeter represented with $x \in (-\pi R_o/2, +\pi R_o/2)$, as shown in Figure 6. Hence, we can simply interpolate the gap function $h(x) = \delta + 2ex/\pi R_o$ with the minimum and maximum gap sizes being $\delta - e$ and $\delta + e$, respectively, and the governing equation for the axial velocity profile $w(x, y)$:

$$0 = -\frac{\partial p}{\partial z} + \mu \frac{\partial^2 w}{\partial y^2}. \tag{18}$$

Of course, we always have the eccentricity between 0 and 1, namely, $0 < e < \delta$. Due to symmetry, we only need to consider half of the width in this case; therefore, the velocity component in the axial (z) direction, satisfying the Dirichlet boundary conditions $w(y) = 0$ at $y = 0$ and $y = h(x)$, can be expressed as follows, which is also stipulated in Ref. [13]:

$$w(y) = \frac{\Delta p}{L_p} \frac{y[h(x) - y]}{2\mu}. \tag{19}$$

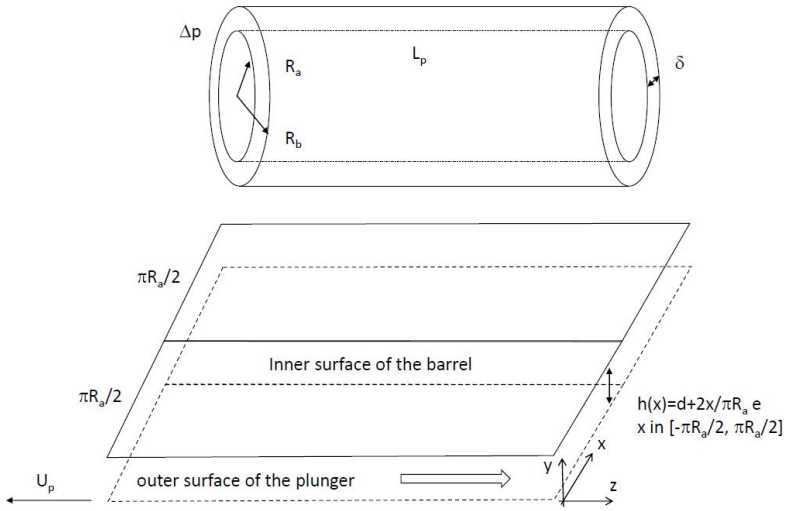


Figure 6. Equivalent annulus fluid domain in Cartesian coordinate system with eccentricity e (adopted from [13]).

Furthermore, we can establish the flow rate Q_p through the annulus region with eccentricity e as $2\int_{-\pi R_o/2}^{+\pi R_o/2}\int_0^{h(x)} w(y)dydx$. The flow rate due to the pressure difference Q_p is then established as follows, with $\epsilon = \delta/R_o$ and the eccentricity evaluated as e/δ:

$$Q_p = \frac{\Delta p}{12\mu L_p} 2\int_{-\pi R_o/2}^{+\pi R_o/2} h(x)^3 dx = \frac{\pi \Delta p}{6\mu L_p} R_o^4 \left[\epsilon^3 + \epsilon^3 (\frac{e}{\delta})^2\right]. \tag{20}$$

Notice that for concentric cases with $e = 0$, the Poiseuille flow rate Q_p derived using the Cartesian coordinate system in Equation (20) matches the leading term derived using the cylindrical coordinate system in Equation (7). Due to the complexity of the problem, as elaborated in [13], the same eccentricity issues have also been studied with computational tools. As confirmed in Figure 7, the computational results match very well with the theoretical predications using Bessel functions in the cylindrical coordinate system and their sinusoidal approximations in the Cartesian coordinate system; more importantly, they also match the results when expanded to cases with eccentricities. Finally, the dynamical behaviors of the sucker rod pump system resembles those of viscoelastic materials, as elaborated in [15,22,27].

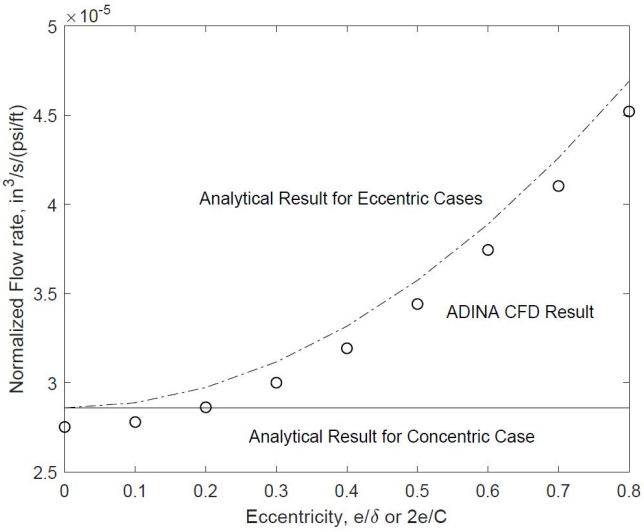


Figure 7. Eccentricity effects on the flow rate through the annulus region (adopted from [13]).

4. Experimental Setup and Validation

The sucker rod experimental setup established in McCoy Engineering Hall at MSU Texas has both horizontal and vertical configurations. Two specific details are important with respect to the horizontal and the vertical configurations. First, in the vertical configuration, the gravitational constant plays an important role in the governing equations. Second, in the vertical configuration, the eccentricity issue can be minimized in comparison with the horizontal configuration. As shown in Figure 2, we have one solenoid valve with four ports and three positions. As depicted in Figure 8, the down-chamber near the cap end corresponds to the sucker rod pump chamber, whereas the up-chamber near the rod end represents the oil well section above the plunger. The tight fit between the plunger and barrel is identical to a sucker rod pump system used in the petroleum industry. In order to simulate the up-stroke, the traveling valve (TV) is replaced with a fixed impermeable end. Furthermore, to ensure a tight seal between the air and liquid, we use the same stuff-box used in the petroleum industry to support the retracting sucker rod that is physically attached to the plunger. In order to measure the sucker rod displacement, an analogue Linear Variable Differential Transformer (LVDT) system is installed at the tip of the sucker rod. Transient pressures within both the down-chamber and up-chamber are measured using a sampling rate from 30 to 120 samples per second or 30 to 120 Hz using the echometer pressure measurement system.

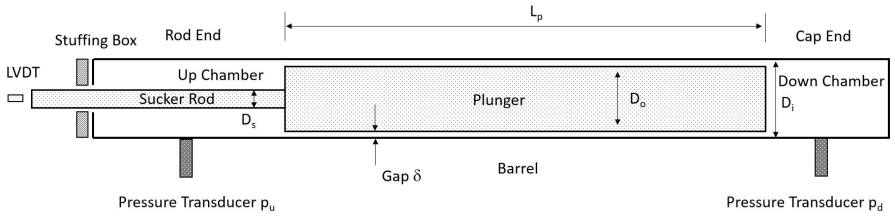


Figure 8. Illustrated details of the sucker rod pump experimental setup (adopted from [15]).

Assuming that the plunger is moving at this time instant with a velocity V_p to the left in a positive direction, as depicted in Figure 4, we have viscous shear force F_v, since one of the external horizontal forces is acting on the plunger from left to right. Furthermore, the pressure in the down-chamber, denoted as p_d, exerts a leftward horizontal force F_d on the plunger, expressed as $p_d \pi R_o^2$, whereas the pressure in the up-chamber, denoted as p_u, exerts a rightward horizontal force F_u on the plunger, expressed as $p_u \pi (R_o^2 - R_s^2)$, where

R_s is the sucker rod radius. Note that in this work we also introduce the gauge pressure; thus, the atmospheric pressure p_{atm} is not added through the cross-sectional area of the sucker rod. Moreover, for the vertical configuration, the gravitational constant g must also be introduced.

Since the plunger is moving from the right to the left at this time instant, as illustrated in Figure 4, the Couette flow Q_c, as the secondary contribution of slippage, is in the same direction; moreover, the Poiseuille flow Q_p due to pressure difference $p_u - p_d$, as the primary contribution of slippage, is from the right to the left. For the Poiseuille flow, as shown in Figure 4, the viscous shear force acting on the plunger surface F_p is also in the negative direction, from the up-chamber to the down-chamber, and can be calculated as in Equation (8). For the Couette flow, as shown in Figure 4, the viscous shear force acting on the plunger surface F_c is in the negative direction, from the up-chamber to the down-chamber, and can be calculated as in Equation (5). Overall, as shown in Figure 4, the flow rate Q from the left to the right is calculated as $Q = Q_p - Q_c$, whereas the shear force to the right is calculated as $F_v = F_c + F_p$.

The following two governing equations are the key to analyzing the experimental data. First of all, we have the kinematic relationship based on the incompressibility of the hydraulic oil and the mass conservation within the cap end. Second, we must observe the dynamical balance of the plunger, or Newton's second law. Assuming the transient rod displacement as U_p (u) and the volume flow rate from the hydraulic pump with power $\bar{P}$, denoted as Q_m, the change of the cap end volume is then depicted as

$$\dot{U}\pi R_i^2 = Q + Q_m, \tag{21}$$

with the transient plunger displacement U_p (abbreviated as U), corresponding velocity V_p (abbreviated as V or $\dot{U}$), and volume flow rate from the hydraulic pump Q_m expressed as $\bar{P}/\Delta p$, or rather $\bar{P}/(p_d - p_u)$.

In this experimental setup, the hydraulic pump has a peak power $\bar{P} = 1$ hp, which is equivalent to 550 lbf $\cdot$ ft/s. Notice that a simpler kinematic relationship holds for the sealed cap end with $Q_m = 0$. Assuming that the total mass of the plunger with the polished rod is m, for the acceleration $\dot{V}$ (or simply a) we have

$$m\dot{V} = F_d - F_u - F_v, \tag{22}$$

where g stands for the gravitational constant, which is only needed for vertical configurations.

Notice here that the pressure measurements p_u in Equation (22) are gauge pressure at both the down-chamber and up-chamber. Therefore, from the kinematic relationship in Equation (21) and utilizing the leading terms in Equations (4) and (7) for viscous flow rates along with Equations (5) and (8) for viscous shear forces, we have

$$V\pi R_o^2 = \frac{p_u - p_d}{6\mu L_p}\pi R_o \delta^3 - V\pi R_o \delta - \frac{\bar{P}}{p_u - p_d} \tag{23}$$

and

$$m\dot{V} = p_d \pi R_o^2 - p_u \pi (R_o^2 - R_s^2) - \pi (p_u - p_d) R_o \delta - 2\pi L_p \mu R_o \frac{V}{\delta}. \tag{24}$$

For the sucker rod experimental setup shown in Figures 2 and 9, we employed MOBIL Hydraulic Oil DTE 24, which has a dynamic viscosity around 1.51569×10^{-2} psi $\cdot$ s. In fact, this particular type of hydraulic oil is widely available in the State of Texas and is currently utilized in our Fluid Power Lab. However, notice that the dynamic viscosity can be sensitive to both impurities and temperature, which suggests a need for further validation with multiple inverse optimization procedures [28]. The plunger length in

the design is 28.5 in with $R_o = 0.615$ in and $R_i = 0.625$ in. Hence, we have clearance of $C = 0.02$ in or $\delta = 0.01$ in or $\epsilon = 0.01626$ with a plunger length $L_p = 4$ in. The polished rod has a radius $R_s = 0.436$ in and length $L_s = 28.5$ in. Finally, in NI LabView measurement, the sensitivity or calibration factor for LVDT measurement in the horizontal configuration is 0.511471 cm/volt or 0.20137 in/volt. In Figure 9, the pressure transducers are connected with the Echometer pressure measurement system. Note that although in engineering practice the sucker rod does not introduce additional viscous shear forces into the pump system, in this experimental setup the gap between the sucker rod radius $R_s = 0.435$ in and the plunger outer radius $R_o = 0.615$ in is sufficiently small, and the viscous shear force due to Couette flow effects can also be estimated as $\mu 2\pi L_s R_o V/\delta$.

As depicted in Figures 9 and 10, the preliminary experimental measures from NI LabView using LVDT and DAQ systems for displacement measurements and pressures in both the up-chamber and down-chamber use Echometer pressure measurement equipment for the horizontal configuration. In this case, the LVDT and Echometer pressure measurement sampling rates are both 30 Hz. Using a heuristic time synchronization method for LVDT and the pressure transducer, we also derived a synchronized set, as illustrated in Figures 11–15.

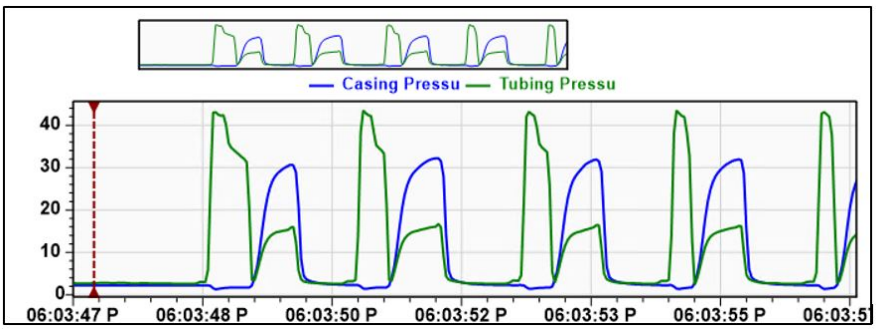


Figure 9. Echometer pressure measurement system for the horizontal configuration (adopted from [15]).

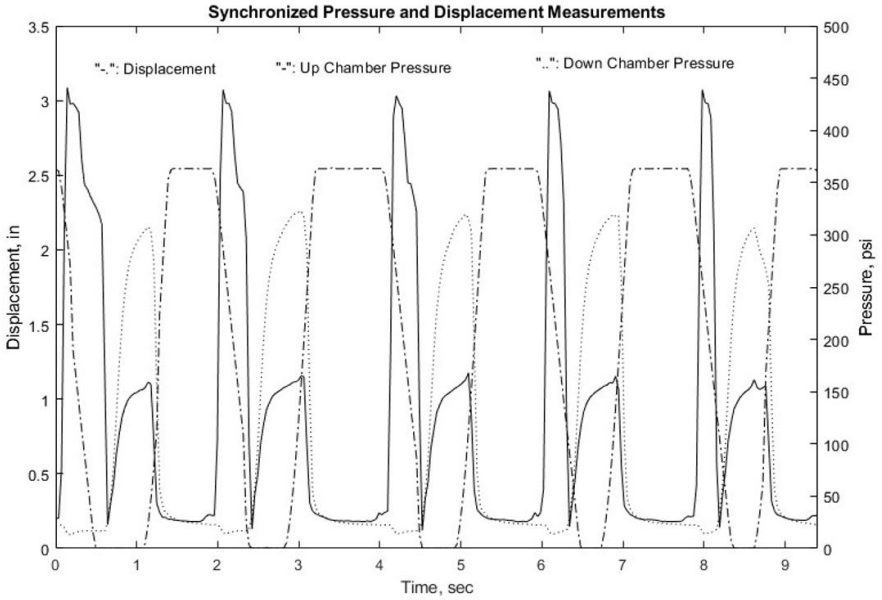
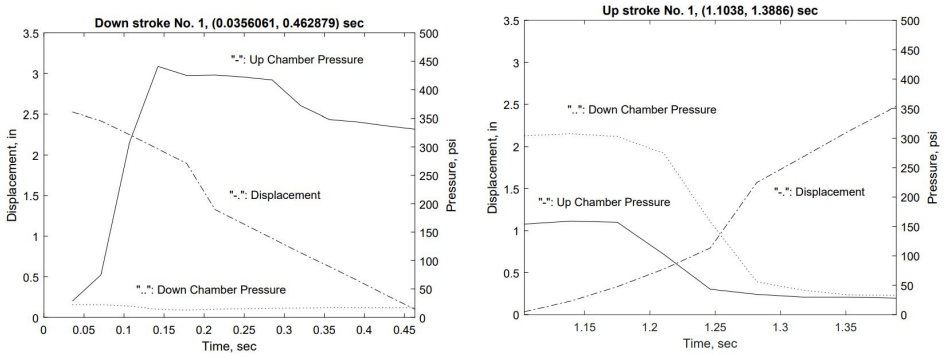
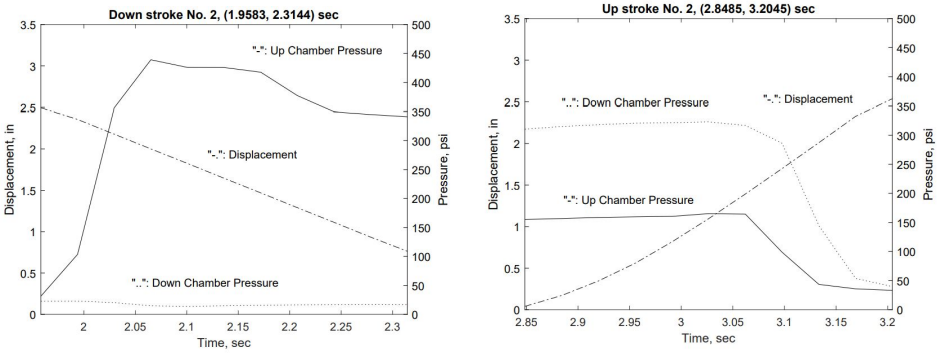


Figure 10. Synchronized pressure and displacement measurements.



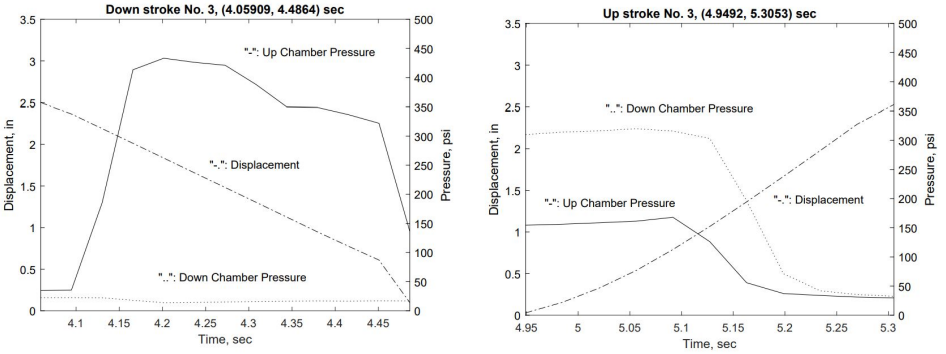
(**a**) Down (**b**) Up

Figure 11. First down- and up-stroke pressure and displacement measurements for the horizontal configuration.



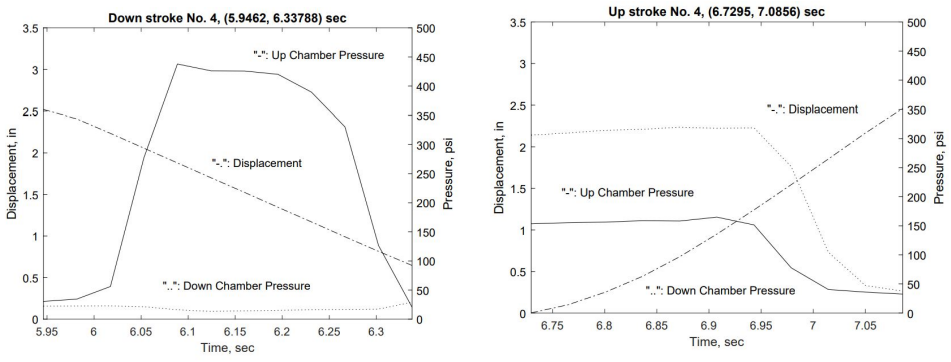
(**a**) Down (**b**) Up

Figure 12. Second down- and up-stroke pressure and displacement measurements for the horizontal configuration.



(**a**) Down (**b**) Up

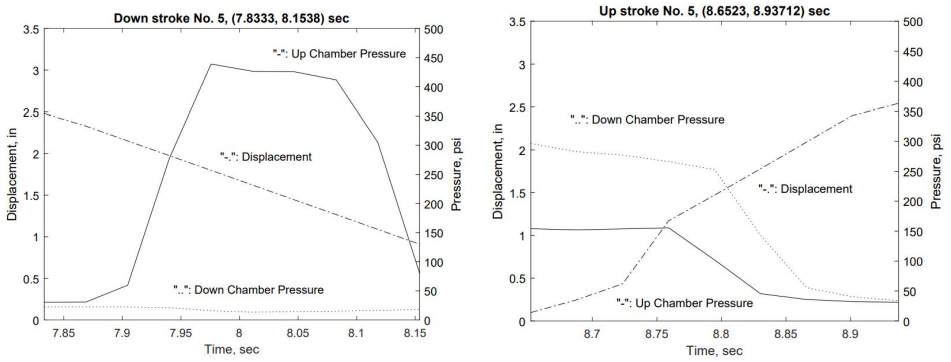
Figure 13. Third down- and up-stroke pressure and displacement measurements for the horizontal configuration.



(**a**) Down (**b**) Up

Figure 14. Fourth down- and up-stroke pressure and displacement measurements for the horizontal configuration.

As illustrated in Figures 12–14, we have identified three fairly consistent sets of down- and up-strokes in which the up-chamber pressure is much higher than the down-chamber pressure for the down strokes, whereas for the up-strokes the down-chamber pressure is much higher than the up-chamber pressure. As a result, the velocity is from the left to the right, which is designated as the negative direction. When the cap end or down-chamber pressure is higher than the rod end or up-chamber pressure, then the rod is pushed to the left. The governing equations are illustrated with Equations (23) and (24), derived using both kinematic and dynamic relationships. For this experimental setup, the plunger length $L_p = 4$ in and the sucker rod length $L_s = 28.5$ in and $\delta = 10$ mil. As shown in Figures 16 and 17, the second, third, and fourth up-strokes demonstrate the consistency of the experimental setup.

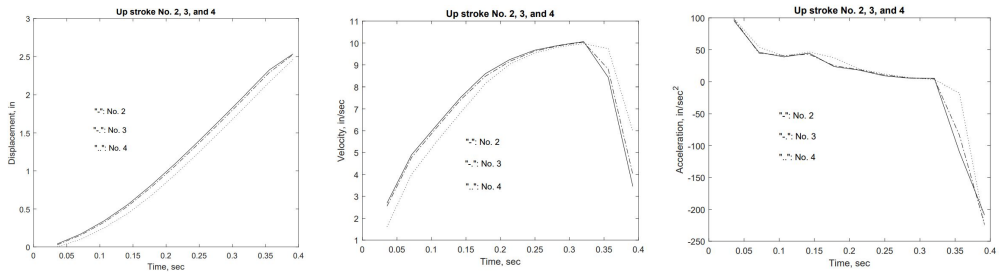


(**a**) Down (**b**) Up

Figure 15. Fifth down- and up-stroke pressure and displacement measurements for the horizontal configuration.

In the following equations, we attempt to utilize the inverse optimization strategy to determine the mass of the sucker rod and the plunger [29]. Inverse optimization methods utilize experimental data to infer unknown parameters for either mathematical models or objective functions with direct error minimizations or optimization [30,31]. The calculated mass is also compared with the physical arrangements. Together with the sucker rod displacement, velocity, and acceleration data from the LVDT measurement, the pressure data obtained from the up-chamber and down-chamber of the system are used to verify the previously-developed theories. Furthermore, we have chosen to utilize the force–balance equation in the vertical direction in an attempt to define

the forces and flow rates related to both the Poiseuille flow and Couette flow within the annulus region between the plunger and the barrel.



(**a**) Displacement (**b**) Velocity (**c**) Acceleration

Figure 16. Second, third, and fourth up-stroke displacement, velocity, and acceleration profiles.

In this research, we employ an inverse optimization method to determine unknown parameters by minimizing errors between experimental data and analytical solutions [32]. Unlike solving a forward (standard) optimization problem, in which system parameters are provided a priori, the inverse optimization method is introduced in this project for multiple reasons. The first advantage is the ability to estimate multiple parameters in complex systems such as sucker rod pump systems [33,34]. Moreover, we can alter the system parameters within the same system to match or predict experimental data. Such an iterative search process can be coupled with the Newton–Raphson methods for nonlinear system.

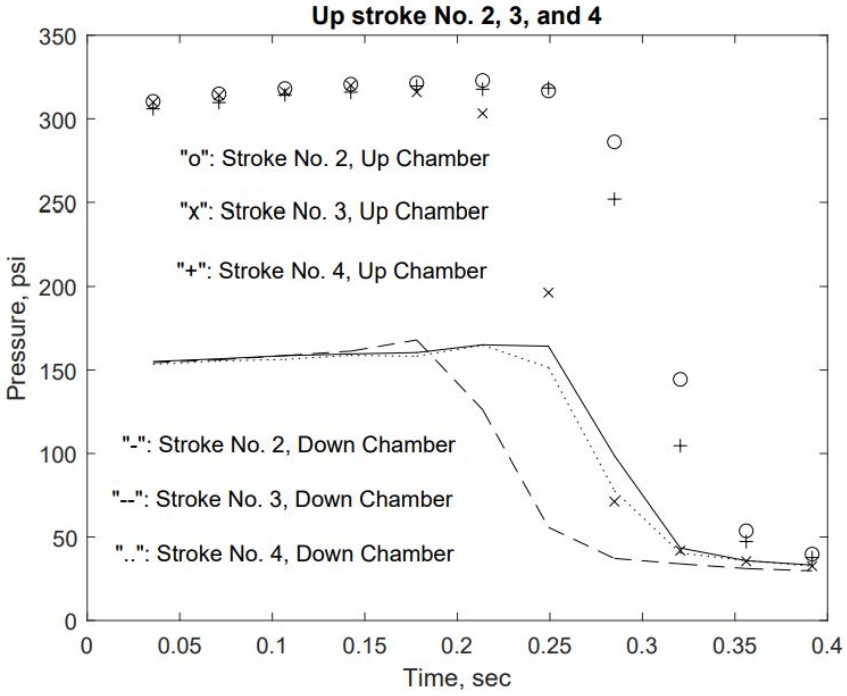


Figure 17. Second, third, and fourth up-stroke pressure profiles for the up-chamber and down-chamber.

Using the free body diagram above, we were able to develop the following equilibrium equation based on Equation (24) for the horizontal configuration:

$$ma = p_d \pi R_o^2 - p_u \pi (R_o^2 - R_s^2) - (p_u - p_d)\pi R_o \delta - 2\mu \frac{V}{\delta} \pi R_o L_p \tag{25}$$

where the upward positive displacement of the plunger is denoted as U, with velocity V, i.e., dU/dt, and acceleration a, i.e., $a = dV/dt$, as presented in Figure 16.

In the inverse optimization procedure with one parameter, the mass m, we start by minimizing the error function E defined with respect to the plunger mass m, as follows:

$$E = \sum_{i=1}^{N} \left[ma_i - p_{d_i} \pi R_o^2 + p_{u_i} \pi (R_o^2 - R_s^2) + (p_{u_i} - p_{d_i}) \pi R_o \delta + 2\mu \frac{V_i}{\delta} \pi R_o L_p \right]^2 \tag{26}$$

where the subscript i stands for the time step number and N is the total number of time steps.

The inverse optimization procedure starts with the minimization of such an error function with respect to the mass m. Thus, for this one-parameter inverse optimization procedure, we have the following equation:

$$\frac{\partial E}{\partial m} = 0.$$

Consequently, we have

$$\sum_{i=1}^{N} a_i \left[ma_i - p_{d_i} \pi R_o^2 + p_{u_i} \pi (R_o^2 - R_s^2) + (p_{u_i} - p_{d_i}) \pi R_o \delta + 2\mu \frac{V_i}{\delta} \pi R_o L_p \right] = 0,$$

which yields $m = b/c$, where the expressions c and b can be evaluated as

$$b = \sum_{i=1}^{N} a_i \pi \left[p_{d_i} R_o^2 - p_{u_i} (R_o^2 - R_s^2) - (p_{u_i} - p_{d_i}) R_o \delta - 2\mu \frac{V_i}{\delta} R_o L_p \right], \quad c = \sum_{i=1}^{N} a_i a_i.$$

However, note the unit conversion from 1 lbf to 32.174 lbm $\cdot$ ft/s^2, or rather 386.1 lbm $\cdot$ in/s^2. For the second up-stroke, we have $c = 17.98$ lbf $\cdot$ in/s^2 and $b = 1021$ in^2/s^4; hence, $m \simeq 6.8$ lbm. As shown in Figure 3, the plunger section has length $L_p = 4$ in and radius $R_o = 0.615$ in along with sucker rod length $L_s = 28.5$ in and radius $R_s = 0.435$ in, as well as a transition section of one inch or so, yielding a total volume of 22.2897 in^3 or total mass of 6.2679 lbm for steel. The close match between the estimated mass based on the inverse optimization method and the actual design volume and mass of the sucker rod and plunger system provides a strong quantitative comparison and validation [35].

In similar experimental setups, it might be difficult to quantify the dynamic viscosity; therefore, it is also possible to follow up with a new inverse optimization procedure with two parameters, namely, the mass m and dynamic viscosity μ. We do this in order to test the model even further and extend our initial validation of the system performance for more accurate prediction of the slippage within the sucker rod pump system. We start with a similar equation to Equation (25) and define the error function E as stipulated in Equation (25) with respect to the plunger mass m and dynamic viscosity μ. Note that multiple system parameters or material constants can be introduced to validate the mathematical models with respective inverse optimization procedures [36,37]. In fact, most inverse optimization procedures are not automatic and must rely heavily on engineers and applied mathematicians' intuition. Hence, in the two-parameter inverse optimization approach we have

$$\frac{\partial E}{\partial m} = 0 \text{ and } \frac{\partial E}{\partial \mu} = 0.$$

Furthermore, we have

$$\begin{aligned} c_1 m + c_2 \mu &= b_1, \\ c_2 m + c_3 \mu &= b_2, \end{aligned}$$

where the expressions c_i and b_i can be evaluated as

$$c_1 = \sum_{i=1}^{N} a_i a_i,\ c_2 = \sum_{i=1}^{N} 2a_i \frac{V_i}{\delta} \pi R_o L_p,\ b_1 = \sum_{i=1}^{N} a_i \pi \Big[p_{d_i} R_o^2 - p_{u_i}(R_o^2 - R_s^2) - (p_{u_i} - p_{d_i}) R_o \delta \Big],$$

$$c_3 = \sum_{i=1}^{N} \left(2\frac{V_i}{\delta} \pi R_o L_p \right)^2,\ b_2 = \sum_{i=1}^{N} 2\frac{V_i}{\delta} \pi^2 R_o L_p \Big[p_{d_i} R_o^2 - p_{u_i}(R_o^2 - R_s^2) - (p_{u_i} - p_{d_i}) R_o \delta \Big].$$

Again using the data for the second up-stroke, we have c_i with $i = 1$ to 3 as 1.021×10^3, 8.758×10^5, and 1.089×10^9, respectively, and b_i with $i = 1, 2$ as 1.693×10^4 and 1.892×10^7, which yields the solutions for m around 5.42573 lbm and for the dynamic viscosity μ around 1.301 psi $\cdot$ s. Similarly, to account for the stiffness effects of the LVDT system, a new error function E with respect to the plunger mass m and stiffness K can be defined as follows:

$$E = \sum_{i=1}^{N} \left[m a_i - p_{d_i} \pi R_o^2 + p_{u_i} \pi (R_o^2 - R_s^2) + (p_{u_i} - p_{d_i}) \pi R_o \delta + 2\mu \frac{V_i}{\delta} \pi R_o L_p + K U_i \right]^2.$$

Again, a similar two-parameter inverse optimization can be introduced with respect to the mass m and spring constant K. Hence, the minimization problem yields

$$\frac{\partial E}{\partial m} = 0 \text{ and } \frac{\partial E}{\partial K} = 0.$$

As a consequence, we have

$$\sum_{i=1}^{N} a_i \left[m a_i - p_{d_i} \pi R_o^2 + p_{u_i} \pi (R_o^2 - R_s^2) + (p_{u_i} - p_{d_i}) \pi R_o \delta + 2\mu \frac{V_i}{\delta} \pi R_o L_p + K U_i \right] = 0,$$

$$\sum_{i=1}^{N} U_i \left[m a_i - p_{d_i} \pi R_o^2 + p_{u_i} \pi (R_o^2 - R_s^2) + (p_{u_i} - p_{d_i}) \pi R_o \delta + 2\mu \frac{V_i}{\delta} \pi R_o L_p + K U_i \right] = 0,$$

which is equivalent to the following linear system equation:

$$\begin{aligned} c_1 m + c_2 K &= b_1, \\ c_2 m + c_3 K &= b_2, \end{aligned}$$

where the expressions c_i and b_i can be evaluated as

$$c_1 = \sum_{i=1}^{N} a_i a_i,\ c_2 = \sum_{i=1}^{N} a_i U_i,\ c_3 = \sum_{i=1}^{N} U_i U_i,$$

$$b_1 = \sum_{i=1}^{N} a_i \pi \left[p_{d_i} R_o^2 - p_{u_i}(R_o^2 - R_s^2) - (p_{u_i} - p_{d_i}) R_o \delta - 2\mu \frac{V_i}{\delta} R_o L_p \right],$$

$$b_2 = \sum_{i=1}^{N} U_i \pi \left[p_{d_i} R_o^2 - p_{u_i}(R_o^2 - R_s^2) - (p_{u_i} - p_{d_i}) R_o \delta - 2\mu \frac{V_i}{\delta} R_o L_p \right].$$

Furthermore, we can also introduce a constant force F to include a constant shift due to the relative displacement for the LVDT measurement and account for the gravitational force in the vertical configuration. Thus, a new error function E can be established with respect to the plunger mass m, stiffness K, and constant force F:

$$E = \sum_{i=1}^{N} \left[m a_i - p_{d_i} \pi R_o^2 + p_{u_i} \pi (R_o^2 - R_s^2) + (p_{u_i} - p_{d_i}) \pi R_o \delta + 2\mu \frac{V_i}{\delta} \pi R_o L_p + K U_i + F \right]^2.$$

For this three-parameter inverse optimization procedure, we derive the following equations:

$$\frac{\partial E}{\partial m} = 0, \quad \frac{\partial E}{\partial K} = 0, \text{ and } \frac{\partial E}{\partial F} = 0.$$

Finally, given that the mass of the sucker rod and the plunger is fairly well documented and calibrated at around 6.8 lbm, we can also focus on the dynamic viscosity, the LVDT-induced stiffness K, and a constant F. Hence, we have the following similar three-parameter inverse optimization procedure:

$$\frac{\partial E}{\partial \mu} = 0, \quad \frac{\partial E}{\partial K} = 0, \text{ and } \frac{\partial E}{\partial F} = 0,$$

$$\sum_{i=1}^{N} 2\frac{V_i}{\delta}\pi R_o L_p \left[ma_i - p_{d_i}\pi R_o^2 + p_{u_i}\pi(R_o^2 - R_s^2) + (p_{u_i} - p_{d_i})\pi R_o\delta + 2\mu\frac{V_i}{\delta}\pi R_o L_p + KU_i + F \right] = 0,$$

$$\sum_{i=1}^{N} U_i \left[ma_i - p_{d_i}\pi R_o^2 + p_{u_i}\pi(R_o^2 - R_s^2) + (p_{u_i} - p_{d_i})\pi R_o\delta + 2\mu\frac{V_i}{\delta}\pi R_o L_p + KU_i + F \right] = 0,$$

$$\sum_{i=1}^{N} \left[ma_i - p_{d_i}\pi R_o^2 + p_{u_i}\pi(R_o^2 - R_s^2) + (p_{u_i} - p_{d_i})\pi R_o\delta + 2\mu\frac{V_i}{\delta}\pi R_o L_p + KU_i + F \right] = 0.$$

Moreover, we have the following linear system of equations:

$$\begin{aligned} c_1\mu + c_2 K + c_3 F &= b_1, \\ c_2\mu + c_4 K + c_5 F &= b_2, \\ c_3\mu + c_5 K + c_6 F &= b_3, \end{aligned}$$

where the expressions for the constants c_i and b_i can be evaluated as

$$\begin{aligned} c_1 &= \sum_{i=1}^{N} (2\frac{V_i}{\delta}\pi R_o L_p)^2, \quad c_2 = \sum_{i=1}^{N} 2\frac{V_i}{\delta}\pi R_o L_p U_i, \quad c_3 = \sum_{i=1}^{N} 2\frac{V_i}{\delta}\pi R_o L_p, \\ c_4 &= \sum_{i=1}^{N} U_i U_i, \qquad c_5 = \sum_{i=1}^{N} U_i, \qquad c_6 = \sum_{i=1}^{N} 1, \end{aligned}$$

$$\begin{aligned} b_1 &= \sum_{i=1}^{N} 2\frac{V_i}{\delta}\pi R_o L_p \left[-ma_i + p_{d_i}\pi R_o^2 - p_{u_i}\pi(R_o^2 - R_s^2) - (p_{u_i} - p_{d_i})\pi R_o\delta \right], \\ b_2 &= \sum_{i=1}^{N} U_i \left[-ma_i + p_{d_i}\pi R_o^2 - p_{u_i}\pi(R_o^2 - R_s^2) - (p_{u_i} - p_{d_i})\pi R_o\delta \right], \\ b_3 &= \sum_{i=1}^{N} \left[-ma_i + p_{d_i}\pi R_o^2 - p_{u_i}\pi(R_o^2 - R_s^2) - (p_{u_i} - p_{d_i})\pi R_o\delta \right]. \end{aligned}$$

Note again that the system is symmetric for this type of minimization problem. Again using the data for the second up-stroke, we obtain c_i with $i = 1$ to 6, as 1.08898×10^9, 1.04965×10^5, 7.36764×10^4, 10.7268, 7.01103, and 5; and b_i with $i = 1$ to 3, as 1.89087×10^7, 1.72462×10^3, and 1.29204×10^3, which yields the solution for the dynamic viscosity μ around 0.13 psi $\cdot$ s and for the constants K and F as -306.1 lbf/in and -977.475 lbf. Note that the negative value of the stiffness K is reasonable, since we assume upward motion and position as positive. It is clear that these data analysis procedures do produce system parameters within the same range. It is also obvious that which inverse optimization procedures should be chosen depends very much on the available information and the feasibility of different physical and mathematical models [38,39]. In fact, throughout the

research on the slippage issues related to sucker rod pump systems it is evident that engineers' physical understanding is essential to the solution of complex engineering problems and the optimization of engineering operations. In the future, comparing both horizontal and vertical configurations can allow us to better identify eccentricity effects. In today's AI-driven economy, although the wealth of information on any engineering problems is at our finger tips, the creative and intuitive understanding of the physics and targeted optimization procedures still depends on individual engineers' professionalism and critical thinking skills.

5. Conclusions

This project represents continuing research towards better understanding and addressing slippage issues in sucker rod pump systems, a flow phenomenon occurring within the annulus region between the barrel and the plunger. Our initial investigations have identified the slippage flow as a combination of Couette flow due to the plunger's reciprocal motions and Poiseuille flow due to the pressure gradient along the plunger's axial length. Earlier research works have identified relaxation times using Bessel functions for cylindrical coordinates as well as by applying Fourier expansion to the Cartesian coordinates, which are much larger than the time step with 30 to 120 samples per second. However, eccentricity issues—which have been partially addressed in the authors' earlier works using perturbation methods and complex flow mechanisms on top of the plunger—mean that much deeper examinations on sucker rod pump systems are still very much needed.

Using a sucker rod pump experimental setup recently established in the McCoy School of Engineering at MSU Texas (a member of the Texas Tech University System), sucker rod displacements can be measured along with the top pressure and bottom pressure of the plunger. In this paper, based on a review of recent computational and analytical studies, we focus our research attention on data analysis of five up- and down-strokes of a horizontal configuration of our experimental setup. We develop one- and multi-parameter inverse optimization procedures based on a theoretical framework established with consideration of system geometries, material properties, and flow characteristics. The experimental setup together with data analysis procedures establishes a strong foundation for better understanding the dynamics of sucker rod pump systems and related slippage issues. The experimental setup is introduced as a physical model to simulate the slippage phenomenon under different yet realistic conditions, complementing and validating our theoretical and computational work. While the physical model represents a critical step towards final verification and validation, in-depth data analysis procedures are still very much needed in order to derive useful information from the wealth of experimental measurements. The data analysis procedures reported in this paper mark a promising start for our future efforts with both vertical and horizontal configurations as well as different system parameters such as overall system damping ratio, sucker rod and plunger mass, overall system stiffness, and dynamic viscosity of hydraulic fluids.

With the feedback provided by this data analysis, a new update will be introduced to the experimental system infrastructure which includes a new pressure filter, enhanced hoses with quick disconnects, and new equipment layouts with improved maintenance accessibility. These modifications will not only streamline our experimental processes but also ensure more reliable and repeatable data acquisition, setting the stage for further analysis of the slippage phenomenon. Finally, for sufficiently wide annulus gaps which sand particles and gas bubbles can squeeze through, further research as depicted in the free Gas Separator Simulator software, presented on the webpage https://www.echometer.com/software, is very much needed in the near future.

Author Contributions: Conceptualization, S.W. and T.C.; methodology, S.W.; software, S.W., C.B., J.T., P.K. and T.C.; validation, S.W., C.B., J.T., P.K. and T.C.; formal analysis, S.W., C.B., J.T., P.K. and T.C.; investigation, S.W., C.B., J.T., P.K. and T.C.; resources, S.W. and T.C.; data curation, S.W., C.B., J.T., P.K. and T.C.; writing—original draft preparation, S.W. and C.B.; writing—review and editing, S.W., C.B., J.T., P.K. and T.C.; visualization, S.W.; supervision, S.W.; project administration, S.W.; funding acquisition, S.W. and T.C. All authors have read and agreed to the published version of the manuscript.

Funding: This research received no external funding.

Institutional Review Board Statement: Not applicable.

Informed Consent Statement: Not applicable.

Data Availability Statement: The original contributions presented in this study are included in the article. Further inquiries can be directed to the corresponding author.

Acknowledgments: We would like to thank faculty and staff members as well as students at Midwestern State University (MSU Texas), a member of the Texas Tech University System, for providing relevant information on this subject and helpful discussion. The professional help from technical staff and engineers at Echometer Company in Wichita Falls, TX are very much appreciated.

Conflicts of Interest: The authors declare no conflict of interest. In particular, Ty Criss was one of the undergraduate students in the McCoy School of Engineering at MSU Texas, a member of the Texas Tech University System. Ty Criss is currently an engineer at Echometer Company. The paper reflects the views of Ty Criss and not the company.

Nomenclature

ρ	fluid density
ν	fluid kinematic viscosity
μ	fluid dynamic viscosity
L_p	plunger length
R_s	sucker rod radius
R_i	inner radius of the barrel
R_o	outer radius of the plunger
δ	gap between the barrel and the plunger
m	total mass of the plunger with sucker rod
z	axial coordinate ($0 \leq z \leq L_p$) for the sucker rod, plunger, and barrel
r	radial coordinate between the plunger (R_o) and the barrel (R_i)
p_u	total pressure on the top of the plunger
p_d	total pressure on the bottom of the plunger
Δp	pressure difference ($p_u - p_d$) over the plunger length (L_p)
$\Delta p / L_p$	negative pressure gradient ($-\partial p / \partial z$) over the plunger length (L_p)
v	axial direction fluid velocity within the annulus flow region
U_p	sucker rod or plunger displacement
V_p	sucker rod or plunger velocity
a	sucker rod or plunger acceleration
g	gravitational acceleration constant
Q_p	Poiseuille flow rate due to the pressure difference
Q_c	Couette flow rate due to the plunger motion
F_p	Poiseuille flow viscous shear force acting on the plunger outer surface
F_c	Couette flow viscous shear force acting on the plunger outer surface

References

1. Karhan, M.K.; Nandi, S.; Jadhav, P.B. Design and Optimization of Sucker Rod Pump Using Prosper. *Int. J. Interdiscip. Res. Innov.* **2015**, *3*, 108–122.
2. Romero, O.J.; Almeida, P. Numerical simulation of the sucker-rod pumping system. *Ing. Investig.* **2014**, *34*, 4–11. [CrossRef]

3. Dong, Z.; Zhang, M.; Zhang, X.; Pang, X. Study on reasonable choice of electric submersible pump. *Acta Pet. Sin.* **2008**, *29*, 128–131.
4. Takacs, G. *Sucker Rod Pumping Manual*; PennWell Corporation: Tulsa, OK, USA, 2003.
5. Podio, A. Artificial Lift. In *Encyclopedia of Life Support Systems*; EOLSS: Paris, France, 2013; pp. 1–9.
6. Yu, Y.; Chang, Z.; Qi, Y.; Xue, X.; Zhao, J. Study of a new hydraulic pumping unit based on the offshore platform. *Energy Sci. Eng.* **2016**, *4*, 352–360. [CrossRef]
7. Wang, S.; Rowlan, L.; Cook, D.; Conrady, C.; King, R.; Taylor, C. Dynamics of pump jacks with theories and experiments. *Upstream Oil Gas Technol.* **2023**, *11*, 100097. [CrossRef]
8. Li, Z.; Song, J.; Huang, Y. Design and analysis for a new energy-saving hydraulic pumping unit. *Proc. IMechE Part C J. Mech. Eng. Sci.* **2017**, *232*, 2119–2131. [CrossRef]
9. Bommer, P.M.; Podio, A.L. *The Beam Lift Handbook*; PETEX: Austin, TX, USA, 2012.
10. Wang, S.; Grejtak, T.; Moody, L. Structural Designs with Considerations of Both Material and Structural Failure. *ASCE Pract. Period. Struct. Des. Constr.* **2017**, *22*, 04016025. [CrossRef]
11. Wang, S.; Yang, Y.; Wu, T. Model Studies of Fluid-Structure Interaction Problems. *Comput. Model. Eng. Sci.* **2019**, *119*, 5–34. [CrossRef]
12. Bommer, P.M.; Podio, A.L.; Carroll, G. The Measurment of Down Stroke Force in Rod Pumps. In Proceedings of the Sixty Third Annual Meeting of the Southwestern Petroleum Short Course, Lubbock, TX, USA, 20–23 April 2016.
13. Wang, S. Scaling, Complexity, and Design Aspects in Computational Fluid Dynamics. *Fluids* **2021**, *6*, 362. [CrossRef]
14. Wang, S.; Rowlan, L.; Elsharafi, M.; Ermila, M.; Grejtak, T.; Taylor, C. On Leakage Issues of Sucker Rod Pumping Systems. *ASME J. Fluids Eng.* **2019**, *141*, 111201.
15. Wang, S.; Rowlan, L.; Henderson, A.; Aleman, S.T.; Creacy, T.; Taylor, C. Viscoelastic representation of the operation of sucker rod pumps. *Fluids* **2021**, *7*, 70. [CrossRef]
16. Rowlan, O.L. (Echometer Company, Wichita Falls, TX, USA); McCoy, J.N. (Echometer Company, Wichita Falls, TX, USA); Lea, J.F. (PL Tech, LLC, Lubbock, TX, USA). Use of the Pump Slippage Equation to Design Pump Clearances. Private communication, 2012.
17. Patterson, J.; Chambliss, K.; Rowlan, L.; Curfew, J. Fluid Slippage in Down-Hole Rod-Drawn Oil Well Pumps. In Proceedings of the 54th Southwestern Petroleum Short Course, Lubbock, TX, USA, 20–23 April 2007; pp. 45–59.
18. Lea, J.F. *What's New in Artificial Lift?* Part I; World Oil: Houston, TX, USA, 2012; pp. 79–85.
19. Zhao, R.; Zhang, X.; Liu, M.; Shi, J.; Su, L.; Shan, H.; Sun, C.; Miao, G.; Wang, Y.; Shi, L.; et al. Production Optimization and Application of Combined Artificial-Lift Systems in Deep Oil Wells. In Proceedings of the SPE Middle East Artificial Lift Conference, Manama, Bahrain, 30 November–1 December 2016; SPE-184222-MS.
20. Falcon, C.; Blanco, C.; Estumano, D. Parameter Estimation Using the Inverse Problem Method for Simulating Lateral Inflow and Runoff Depth in a small catchment of Amazon. *Ann. Braz. Acad. Sci.* **2024**, *96*, e20230570. [CrossRef] [PubMed]
21. Mamlankou, C. Inverse Problem Analysis in the Dynamics of Damped Harmonic Oscillators Using Pinns. *Hal Open Sci.* **2025**, *preprint*; HAL Id: hal-04949890.
22. Wang, S.; Gao, D.; Wester, A.; Beaver, K.; Edwards, S.; Taylor, C. Pump System Model Parameter Identification Based on Experimental and Simulation Data. *Fluids* **2024**, *9*, 136. [CrossRef]
23. Tarantola, A. *Inverse Problem Theory and Methods for Model Parameter Estimation*, 3rd ed.; SIAM: Philadelphia, PA, USA, 2005.
24. Lieberman, C.; Willcox, K.; Ghattas, O. Parameter and State Model Reduction for Large-scale Statistical Inverse Problems. *SIAM J. Sci. Comput.* **2010**, *32*, 2523–2542. [CrossRef]
25. Wu, Y.; Wu, X.; Wang, Y.; Yuan, Y. A New Eccentric Annular Leakage Model for Rod Pump with Couette-Poiseuille Flow. *Int. J. Control Autom.* **2013**, *6*, 289–302.
26. Wang, S. *Fundamentals of Fluid-Solid Interactions-Analytical and Computational Approaches*; Elsevier Science: Amsterdam, The Netherlands, 2008.
27. Wang, S.; Gao, D.; Pouraria, H. Fluid-Structure interaction effects on developing complex non-Newtonian flows within flexible tubes. *Fluids* **2025**, *10*, 210. [CrossRef]
28. Rao, P. Inverse parameter estimation using compressed sensing and POD-RBF reduced order models. *Comput. Methods Appl. Mech. Eng.* **2024**, *422*, 116820. [CrossRef]
29. Chan, T.; Mahmood, R.; Zhu, I. Inverse Optimization: Theory and Applications. *Oper. Res.* **2023**, *73*, 1046–1074. [CrossRef]
30. Aster, R.; Borchers, B.; Thurber, C. *Parameter Estimation and Inverse Problems*, 3rd ed.; Elsevier: Amsterdam, The Netherlands, 2018.
31. Bertero, M.; Boccacci, P. *Introduction to Inverse Problems in Imaging*, 1st ed.; CRC Press: Boca Raton, FL, USA, 2020.
32. Jacob, D. *Lectures on Inverse Modeling*; Harvard University: Cambridge, MA, USA, 2007.
33. Cronert, T.; Martin, L.; Minner, S.; Tang, C. Inverse optimization of integer programming games for parameter estimation arising from competitive retail location selection. *Eur. J. Oper. Res.* **2024**, *312*, 938–953. [CrossRef]

34. Kasai, R.; Al-Ola, O.A.; Yoshinaga, T. Coupled Dynamical Systems for Solving Linear Inverse Problems. *Mathematics* **2025**, *13*, 3347. [CrossRef]
35. Johnson, M.; Aghasadeghi, N.; Bretl, T. Inverse optimal control for deterministic continuous-time nonlinear systems. In Proceedings of the 52nd IEEE Conference on Decision and Control, Florence, Italy, 10–13 December 2013; pp. 2906–2913.
36. Zanni, L.; Benfenati, A.; Bertero, M.; Ruggiero, V. Numerical Methods for Parameter Estimation in Poisson Data Inversion. *J. Math. Imaging Vis.* **2014**, *52*, 397–413. [CrossRef]
37. Flavien, A.; Mansour, D.; Mazen, S. Joint state-parameter estimation and inverse problems governed by reaction–advection–diffusion type PDEs with application to biological Keller–Segel equations and pattern formation. *J. Comput. Appl. Math.* **2025**, *461*, 116454. [CrossRef]
38. Hosseiniiraj, E. Inverse Parametric Optimization for Learning Utility Functions from Optimal and Satisfising Decision. Ph.D. Thesis, Concordia University, Montreal, QC, Canada, 2021
39. Farquharson, C.; Oldenburg, D. A comparison of automatic techniques for estimating the regularization parameter in nonlinear inverse problems. *Geophys. J. Int.* **2004**, *156*, 411–425. [CrossRef]

Disclaimer/Publisher's Note: The statements, opinions and data contained in all publications are solely those of the individual author(s) and contributor(s) and not of MDPI and/or the editor(s). MDPI and/or the editor(s) disclaim responsibility for any injury to people or property resulting from any ideas, methods, instructions or products referred to in the content.